Theoretical and Applied Fracture Mechanics 119 (2022) 103341

Contents lists available at ScienceDirect

Theoretical and Applied Fracture Mechanics

journal homepage: www.elsevier.com/locate/tafmec

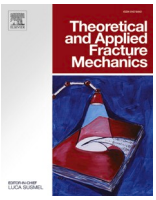

Crack initiation and slow growth in soda-lime glass from a self-healed crack

S. Dondeti, H.V. Tippur *

Department of Mechanical Engineering, Auburn University, AL 36849, USA

ARTICLE INFO

Keywords:
Soda-lime glass
Crack healing
Slow crack growth
Quantitative visualization
Finite element simulation

ABSTRACT

Soda-lime glass (SLG) is a widely used structural material with many advantages in terms of thermal, physical and mechanical properties besides esthetics, sustainability and environmental impact. As a highly brittle, low-toughness and high-stiffness material, understanding its failure behavior in general and fracture mechanics in particular is critical for structural applications. The propensity for hairline crack formation at stress concentration sites during service is particularly a critical issue. Hairline cracks in SLG can occasionally heal when the structure is unloaded, become optically invisible and go undetected, causing unexpected and catastrophic failure upon reloading. In this work, crack initiation and quasi-static crack growth from a self-healed crack in SLG plate is recreated and investigated under laboratory conditions. A wedge-splitting test (WST) geometry is adopted to carry out the study. A pre-cut notch is loaded using a wedge to generate a hairline crack and let to heal without any external stimulus. An opto-mechanical study of crack (re)initiation and growth is carried out while mapping the crack-tip stress gradients in the whole field using the transmission-mode Digital Gradient Sensing (DGS) method. An abrupt re-initiation and extension of the self-healed crack, subsequent initiation of the natural crack-tip followed by a slow crack growth are all captured by the far-field load–displacement response as well as the local crack-tip fields. The stress intensity factor (SIF) history for the entire event is extracted subsequently. The results indicate approx. 50% lower value of critical SIF at re-initiation of the self-healed crack relative to the natural/virgin crack. The crack growth resistance behavior shows a nominally constant energy release rate of 6.5 $\pm$ 0.5 J/m^2 during slow crack growth. A companion finite element (FE) model that mimics optical measurements is also included. The simulations suggest that the contact stiffness of the self-healed crack is about 60% of the virgin material.

1. Introduction

During service, cracks tend to initiate and grow in regions of high stress concentration in a structure. In high stiffness and low toughness brittle structural materials such as soda-lime glass (SLG), hairline cracks emanating from stress concentrations can occasionally heal back [1–3] upon unloading. Such self-healed cracks are optically invisible and can go undetected, making structures highly vulnerable to premature and catastrophic failure during subsequent overload cycles. In this context, crack initiation and crack growth from a self-healed crack in soda-lime glass is important to understand and hence investigated in this work.

The slow crack growth in soda-lime glass is said to occur in three characteristic phases [4–6]. In the first phase, the crack velocity dependence on stress intensity factor is governed by an exponential relationship. In the second phase, the crack velocity is said to be nearly independent of the stress intensity factor. After an increase of stress intensity factor, higher crack velocity occurs in the third phase, followed by an unstable crack propagation. Both first and second phases are considered slow (subcritical) crack growth regimes. Wiederhorn and Townsend [1,4,6] were among the early investigators to examine slow crack growth in self-healed soda-lime glass plates. They generated cracks in double cantilever beam specimens and observed crack closures upon unloading. The closure was attributed to partial reestablishment of chemical bonds between the newly formed surfaces. Their results indicated a lower stress intensity factor and surface energy for self-healed cracks when compared to unhealed cracks. The critical stress intensity factor and fracture surface energy for self-healed crack was reported by them as 0.17 MPa$\sqrt{\text{m}}$ and 0.2 $\pm$ 0.2 J/m^2, respectively. This was significantly lower relative to the critical stress intensity factor of the virgin material, at $\sim$ 0.76 MPa$\sqrt{\text{m}}$, indicating substantial diminution of fracture toughness of SLG due to a self-healed crack relative to the virgin material. They also reported that the critical stress intensity factor increased with an increase in relative humidity (RH). Michalske et al., [2] investigated self-healed cracks in soda-lime glass using double

* Corresponding author.
E-mail address: tippuhv@auburn.edu (H.V. Tippur).

https://doi.org/10.1016/j.tafmec.2022.103341
Received 17 January 2022; Received in revised form 23 February 2022; Accepted 28 March 2022
Available online 29 March 2022

cleavage drilled-hole compression (DCDC) specimens. They reported strain energy release rate for crack closure to be 0.15 J/m^2. Their results also showed that the healed cracks required more energy to reopen (at a RH < 50%) when compared to crack closure counterparts. At RH > 50%, the amount of strain energy release rate required for reopening of healed cracks was almost same as that for crack closure. Due to challenges associated with achieving controlled slow crack growth in a highly brittle material such as soda-lime glass, very few works can be found on this topic in the subsequent literature. Recently, To et al., [7] have revisited slow crack growth in SLG. They have successfully created pre-cracks in a beam using a bridge-flexure method and conducted three-point bend experiments on specimens with healed cracks to evaluate the critical stress intensity factors. Similar to prior works, they have employed far-field applied loads to quantify the local fracture parameters.

Despite the availability of a number of sophisticated full-field interferometric and vision-based techniques, very few optical investigations on this topic can be found in the literature due to extreme sensitivity requirements to study SLG. An exception in this regard is a report by Ferretti et al., [8]. These authors examined intriguing questions concerning inelastic (plastic) crack-tip deformations in annealed soda-lime glass. Using electronic speckle pattern interferometry they evaluated the crack opening displacements near a stationary natural crack grown ahead of a notch in a beam. Their measurements suggest the presence of a bulk process zone confined to the crack-tip vicinity. A numerical analysis employing the finite element method and Gurson-like material model to account for microvoids and microcracks matched measurements better than LEFM and cohesive zone models. In another study, Singh et al., [9] optically investigated crack growth in a glass. They adopted holographic interferometry to monitor crack growth. By using Fourier transform-based fringe analysis and phase-unwrapping methods, the crack location was identified. However, no quantification of fracture parameters is reported in their work. Sundaram and Tippur [10] were the first to demonstrate the feasibility of a relatively new optical method called digital gradient sensing (DGS) to quantitatively visualize *two* orthogonal stress gradients near a *stationary* crack and extract fracture parameters in SLG. They have also demonstrated the feasibility of this method to study fast fractures (crack speeds of ~ 1500 m/s) including the crack branching phenomena [11–13].

A wedge splitting test (WST) geometry has been used by many investigators to achieve slow crack growth in ultra-brittle materials including cementitious and geomaterials [14,15]. This geometry enables controlled slow crack propagation using a relatively small force applied in a standard testing machine [14]. Brühwiler et al., [15] and Korte et al., [16] used WST geometry to study stable fracture in concrete and evaluate fracture parameters. Walter et al., [17] investigated steel–concrete interfaces using a WST configuration and determined fracture parameters. Slow crack propagation in commercial refractory materials has also been studied using this method. Vargas et al., [18] evaluated fracture parameters using WST geometry and digital image correlation (DIC). Dai et al., [19] used WST configuration to study quasi-brittle magnesia refractories. They evaluated crack lengths in magnesia and magnesia spinel materials during cyclic loading of WST specimens based on the localized strains evaluated using DIC. The refractory materials that showed reduced brittleness were found to consume a small amount of energy for crack initiation but a large amount of energy for subsequent crack propagation.

In the present study, initiation of a self-healed crack and slow growth in soda-lime glass is investigated by directly quantifying the fracture parameters from measured crack-tip stress fields. For this purpose, the full-field optical method, DGS, is used. To achieve slow crack growth in soda-lime glass, the WST configuration is employed. By using DGS method along with an over-deterministic least-squares analysis of measurements, the mode-I stress intensity factors and fracture energy release rates are quantified. A companion finite element analysis is also carried out to supplement the optical measurements. In the following, first the experimental details pertaining to the specimen geometry, optical method, experimental setup, post-processing of measurements, and extraction of fracture parameters are presented. Next, details concerning a companion finite element modeling effort guided by the optical measurements follow. A discussion of results including potential sources of errors due to ultrahigh sensitivity measurements is presented subsequently followed by major conclusions.

2. Materials and methods

2.1. Specimen geometry

SLG specimens were machined from a 5.7 mm thick, commercially procured sheet into the Wedge Splitting Test (WST) specimens illustrated in Fig. 1. A 10 mm long notch was cut into the specimen using a 300 μm thick diamond impregnated circular-saw. To generate a natural crack in the specimen, a steel wedge was tapped into the machined notch using a mallet while the specimen was resting on its opposite edge on a table-top. This resulted in the generation of a natural crack from the initial notch-tip. Once, the natural mode-I crack was generated, the wedge was retracted and the specimen was rested under laboratory conditions for a few hours before testing. In the interim, the natural crack self-healed, as evident in Fig. 2. Some relevant mechanical and physical properties of soda-lime glass required for this study are listed in Table 1.

2.2. Optical method

A full-field vision-based method called Digital Gradient Sensing (DGS) when used in light transmission-mode has been found to be highly effective in mapping stress gradient fields near stress concentrations [11–13,20]. Sundaram and Tippur [11] were the first to extend DGS to study dynamic fracture in soda-lime glass. Recently, Dondeti and Tippur [12] have undertaken a comparative study of dynamic fracture in soda-lime glass using multiple full-field optical methods namely, photoelasticity, DIC, and DGS. They have shown DGS to be very effective in not only visualizing the crack-tip fields but in quantifying the fracture parameters accurately when compared to others. A more complicated situation involving cascading crack branch formation was also investigated by the same authors to identify multiple fracture mechanics-based precursors associated with the crack branching phenomenon [13].

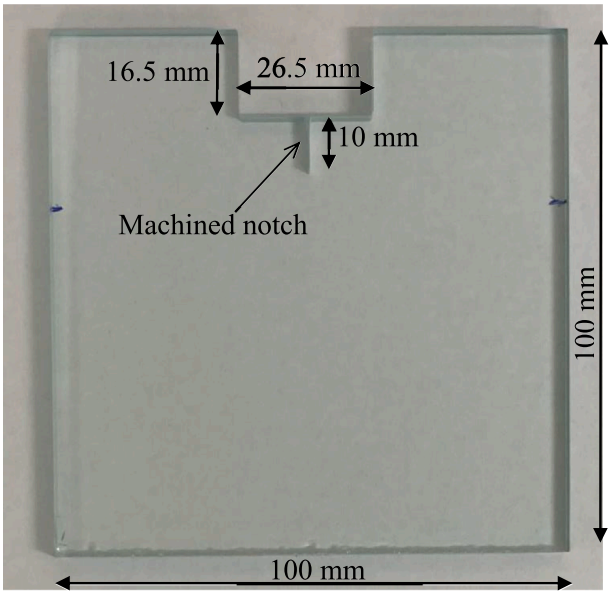

Fig. 1. Wedge Splitting Test (WST) soda-lime glass specimen geometry with machined notch. (Plate thickness = 5.7 mm; notch length = 10 mm).

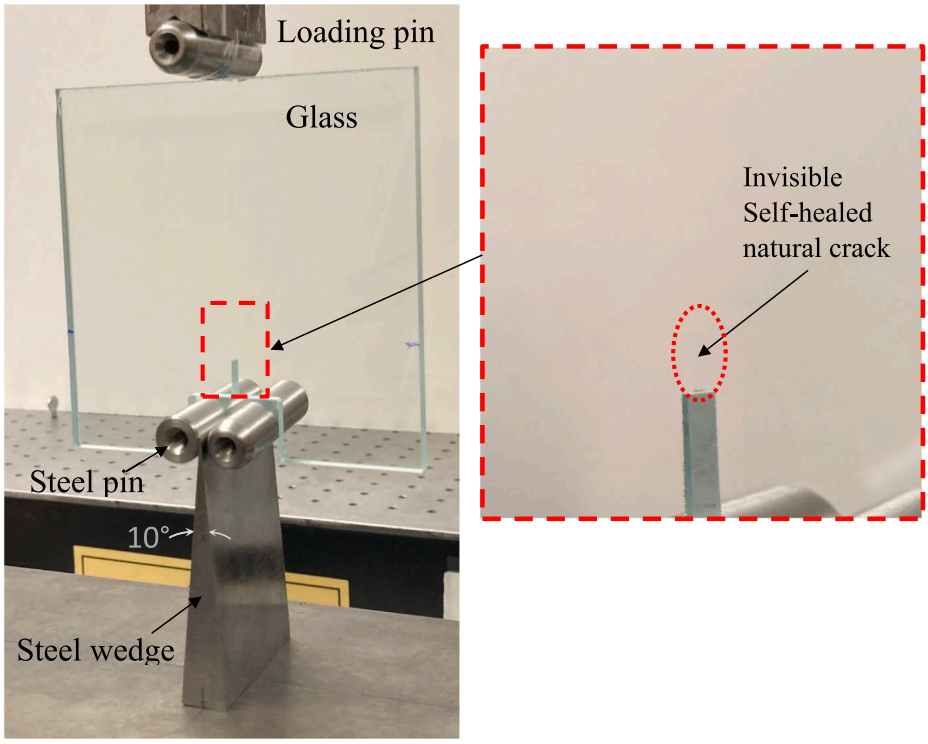

Fig. 2. WST (Wedge Splitting Test) specimen loading configuration. Notice the lack of evidence of the healed-crack emanating from the notch-tip.

Table 1
Some relevant soda-lime glass properties.

Property	Value
Density, ρ	2500 kg/m^3
Elastic modulus, E	70 GPa
Poisson's ratio, υ	0.22
Tensile strength, σ_t	41–180 MPa
Compressive strength, σ_c	330 MPa
Elasto-optic constant, C_σ	-0.027×10^{-10} m^2/N
Stress-optic constant, f_σ	0.22 MPa-m/fringe

Though DGS has been used previously for studying fast fracture events in SLG, its applicability to slow and subcritical crack growth is yet to be demonstrated. The extremely small deformations during subcritical crack growth makes it a rather challenging task as crack growth is known to occur at much lower values of stress intensity factors relative to the fracture toughness of SLG. DGS technique [20] was attempted in this work to visualize and quantify crack-tip fields associated with crack initiation and growth of a self-healed crack and subsequent initiation at the natural crack-tip followed by slow crack growth phenomena.

DGS utilizes digital image correlation to quantify perceived/pseudo speckle shifts that are proportional to orthogonal in-plane stress gradients when observed through planar specimens. A random speckle decoration on a planar surface, called a 'target', is illuminated using ordinary polychromatic lamps and photographed through the region-of-interest (ROI) in the specimen, see Fig. 3. The gray scale is photographed first in the reference state when a point P on the target plane (x_0-y_0 plane) is recorded through a point O on the specimen plane (x-y plane). Upon loading, the non-uniform state-of-stress in the specimen alters the refractive index and the thickness locally, say, in the crack-tip vicinity. This phenomenon, commonly referred to as the elasto-optic effect, makes the light rays to deviate from their original path as they propagate through the stressed specimen. The gray scale photographed through the specimen in the stressed state results in recording of a neighboring point Q on the target through the same point O on the specimen. By correlating the speckle images in the reference (unstressed) and stressed states, pseudo-shifts in speckle clusters, δ_x and δ_y, can be quantified by correlating the images. Knowing the distance between the specimen and the target planes from the experimental setup, the angular deflections of the light rays ϕ_x and ϕ_y in two orthogonal planes (x-z and y-z planes, the z-axis coinciding with the optical axis of the setup and x-y being the specimen plane coordinates) can be evaluated simultaneously. These angular deflections are proportional to the gradients of the in-plane normal stresses as,

$$\phi_{x;y} = \pm C_\sigma B \frac{\partial(\sigma_x + \sigma_y)}{\partial x; y} \tag{1}$$

where C_σ is the elasto-optic constant of the material, B is its initial thickness, $(\sigma_x + \sigma_y)$ is the first stress invariant under plane stress condition, and σ_x and σ_y denote the thickness-wise averages of Cauchy's normal stress components [20].

It is important to note that while recording speckles, the camera is focused on the target through the transparent specimen. However, to perform analysis of the mechanical fields, they are needed in terms of the specimen plane coordinates. This is achieved by mapping P(x_o, y_o) on the target plane to point O(x, y) on the specimen using the so-called pin-hole camera approximation. The mapping function between the specimen and the target planes is,$(x; y) \times (L + \Delta) = (x_o; y_o) \times L$ where L and Δ represent distances between the camera and the specimen and specimen and the target planes, respectively.

2.3. Experimental setup

A schematic representation of the experimental setup is shown in Fig. 4. A narrow 10° steel wedge along with a pair of ground steel pins were used to support the SLG specimen and subjected to a line-load via another steel pin. The load was applied in a displacement controlled mode using Instron 4465 mechanical testing machine at a crosshead speed of 1 μm/s. A Point Grey Grasshopper3 digital camera with 2048 × 2048 pixels sensor and 18–108 mm focal length zoom lens was used to record speckles on the target plane, through the specimen, at 5 fps. The target plane was located behind the specimen plane at a distance of ~

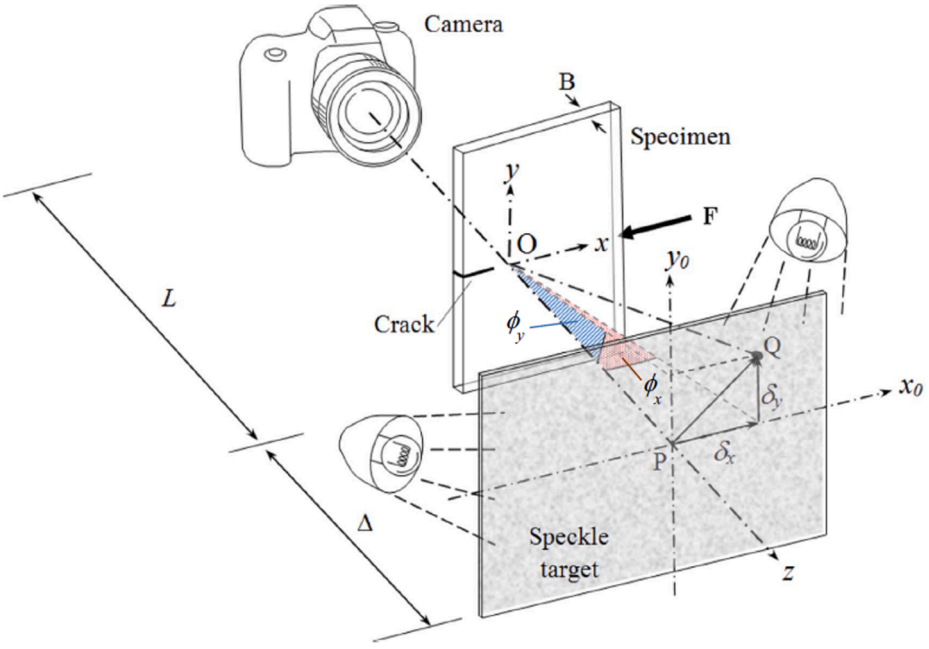

Fig. 3. Schematic of Digital Gradient sensing (DGS) technique to determine planar stress gradients.

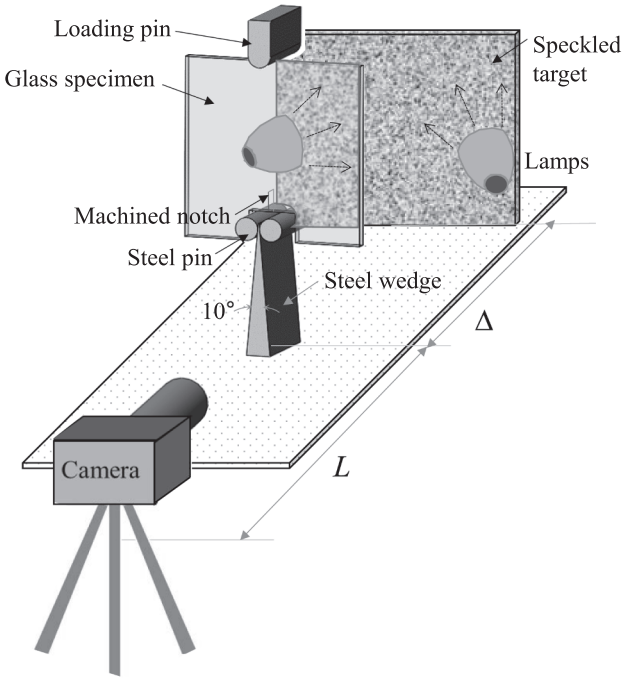

Fig. 4. Schematic of DGS experimental setup with WST specimen geometry.

0.6 m and the camera was at ~ 0.9 m ahead of the specimen plane. The ROI in this experiment covered all the events including initiation and growth of the self-healed crack as well as the natural crack. A 141 × 141 mm^2 region covered by random speckles on the target, corresponding to approx. 84 × 84 mm^2 on the specimen, was photographed. The resulting magnification factor (or, the scale factor) of these images was 69 μm/pixel. Assuming a speckle shift sensitivity of approx. 1% of the magnification factor, an angular deflection accuracy of about 10 μrad was expected.

The load–displacement plot recorded by the load-cell of the testing machine is shown in Fig. 5(a). The load increased monotonically until crack initiation. (The initial loading phase was nonlinear due to the

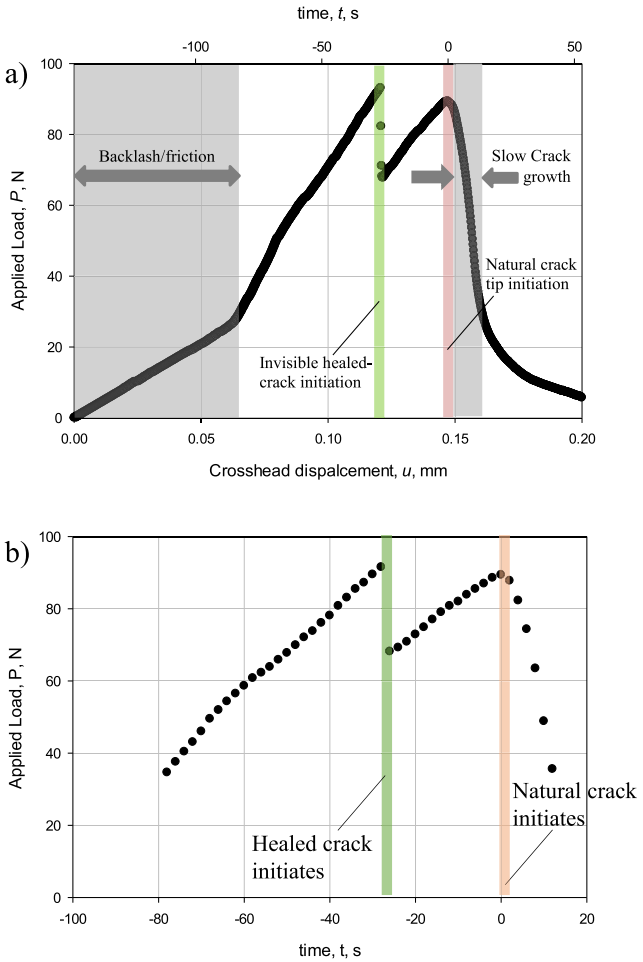

Fig. 5. Far-field measurements: (a) Load-displacement record from the testing machine and (b) Load history corresponding to fracture parameters evaluated using DGS (data at every 2 s time step was considered, Time, $t = 0$ corresponds to crack initiation at natural crack tip).

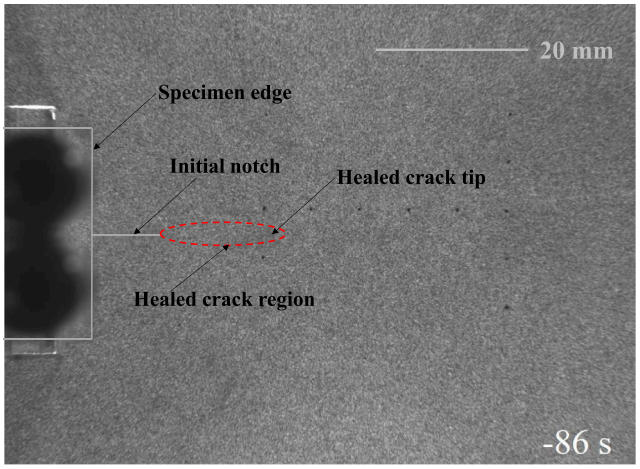

Fig. 6. Photograph of a typical speckle image recorded by camera through the soda-lime glass specimen with initial notch.

backlash in the loading screw and friction at multiple contact pairs, Fig. 5(a).) Once the healed crack initiated at ~ 92 N, the load dropped instantaneously to ~ 71 N. Subsequently, the load increased linearly to a value of ~ 88 N until initiation of the natural hairline crack that had previously healed. Later, a slow crack growth in the specimen resulted in a more gradual reduction of load, as highlighted in Fig. 5(a). (Fig. 5(a) also shows the recorded load histories with horizontal axis as time, *t*, on top of the chart.) As expected, both the load–displacement plot and the load history show similar trends due to the constant loading rate used during the test. For analyzing the optical data, images and hence load/deflection data at every 2 s intervals were considered to reduce the amount of post-processing of full-field optical data. Accordingly, the load–displacement plot corresponding to the reduced data set is shown in Fig. 5(b).

2.4. Stress gradients

A speckle image in the early stages of loading of the specimen with the self-healed crack is shown in Fig. 6. The specimen edge, initial notch, healed crack region and natural crack-tip location are all identified in the figure. A photograph of the fractured specimen from this experiment is also shown in Fig. 7. During the experiment, the crack initiated from the self-healed notch-tip after it opened suddenly while loading at a constant rate. Subsequently, the crack initiated at the original hairline crack-tip, produced during wedge insertion step, and it propagated slowly in a mode-I condition.

The angular deflections of light rays, ϕ_x andϕ_y, in two orthogonal directions (with respect to the propagating mode-I mother crack) at select time instants, are shown in Fig. 8 as contour maps. These contour maps were obtained by segmenting the target plane speckle images in the reference and deformed states of the specimen, recorded at different time instants, into 60 × 60 pixel sub-images. The location of a sub-image in the deformed state was determined relative to its position in the reference state by performing 2D gray scale correlation using the image analysis software ARAMIS® (GOM mbH, Braunschweig, Germany). An overlap of 10 pixels was used during analysis. Once the location of a sub-

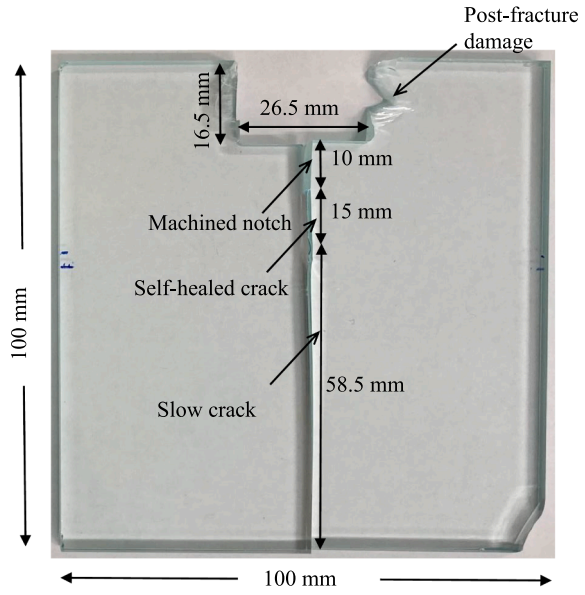

Fig. 7. Photograph of fractured WST specimen. (Visible damage to edges are due to collision of fractured pieces with equipment in the post-fracture phase).

image in the deformed state was identified, the local speckle shifts were quantified at the center of each sub-image. This resulted in data arrays of pseudo speckle shifts corresponding to horizontal and vertical directions, δ_x and δ_y, respectively. Each of these arrays were 178 × 198 in size. These were subsequently converted into ϕ_x and ϕ_y fields by dividing speckle shifts by the gap Δ between the specimen and target planes in the optical setup. The first column in Fig. 8 represents contours of ϕ_x and ϕ_y for the initial notch-tip (before the self-healed crack opened) at time $t = -32$ s whereas the second column correspond to the natural crack-tip fields (after the healed crack opened) at time $t = -20$ s. Here, *the timestamps are with respect to the instant when the crack initiated at the natural crack-tip due to wedge insertion, identified as* $t = 0$. The ϕ_x contours are symmetric relative to the dominant mode-I crack path whereas ϕ_y contours are antisymmetric. Locating the crack-tip from these DGS contours is rather straightforward due to the singular nature of the two stress gradient fields [12]. That is, the contours representing each of the measured fields have closed-lobe structures converging at the crack-tip, marked in Fig. 8 by a solid white dot/circle, making it relatively easy to locate it at each time instant or load-step from either of the two fields. That is, as can be seen from Fig. 8, once the contours are plotted via post-processing, the instantaneous crack-tip position becomes self-evident.

2.5. Stress intensity factor history

The mode-I SIFs were then evaluated by analyzing the angular deflections ϕ_x around the crack-tip in conjunction with the asymptotic equation [10] using an over-deterministic least-squares error minimization approach using the asymptotic stress gradient field expression,

$$\phi_x = C_\sigma B \frac{\partial(\sigma_x + \sigma_y)}{\partial x} = C_\sigma B \left[-\frac{1}{2} r^{-\frac{3}{2}} \left\{ A_1 cos\left(\frac{3\theta}{2}\right) \right\} + \sum_{N=2}^{\infty} \left(\frac{N}{2} - 1\right) r^{\left(\frac{N}{2}-2\right)} \left\{ A_N \cos\left(\left(\frac{N}{2} - 2\right)\theta\right) \right\} \right] \quad (2)$$

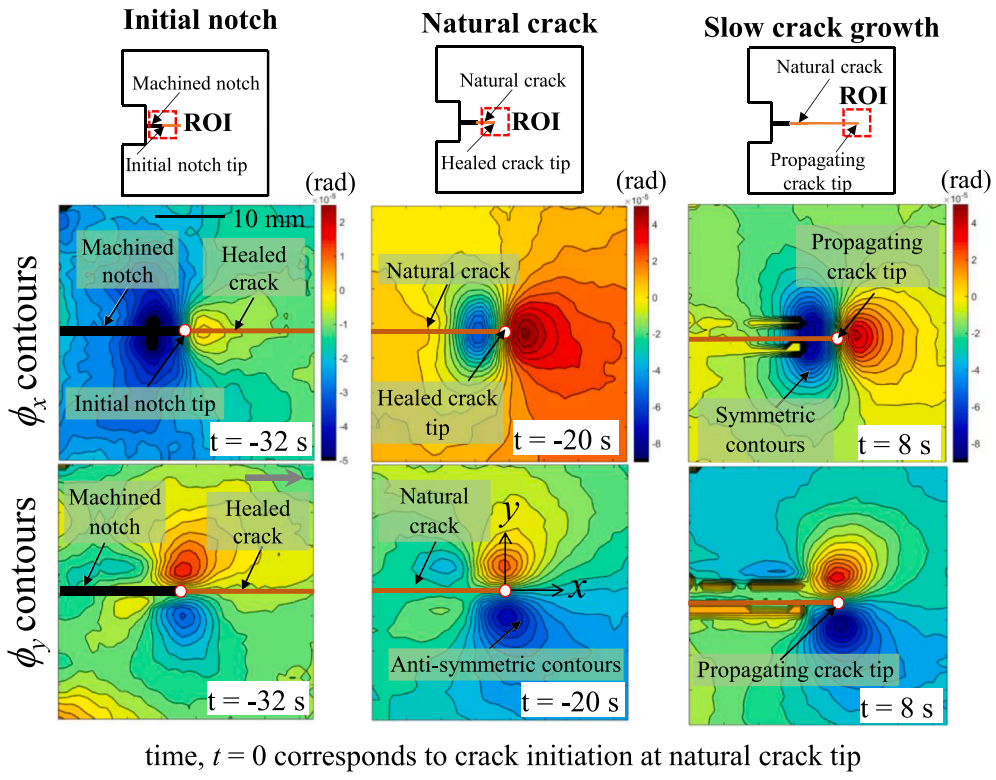

Fig. 8. Contours of angular deflections of light rays (contour increment = 5×10^{-6} rad) in WST soda-lime glass plate with a self-healed crack measured using DGS. The arrowhead (in the bottom left image) shows crack growth direction.

In the above, (r, θ) denote the local crack-tip polar coordinates, and $r = \sqrt{x^2 + y^2}$ and $\theta = tan^{-1}\left(\frac{y}{x}\right)$ in the crack growth direction. The coefficient A_1 in the asymptotic series are related to the mode-I SIF, as$K_I = A_1\sqrt{\frac{\pi}{2}}$. For analysis purposes, the data near the crack-tip region with an angular extent of $-150° \leqslant \theta \leqslant 150°$ but different radial extents was considered. The least-squares analysis was performed with four ($N = 3$) terms in the asymptotic stress field expressions and was guided by previous works [1,2]. In Eq. (2), C_σ is the elasto-optical constant for SLG, and B is the nominal plate thickness.

The crack speed was first extracted from the optical measurements and are plotted in Fig. 9(a). Evidently, the crack speeds are very low, maximum being approx. 3.5 mm/sec. Furthermore, the velocity from the virgin/natural crack increases gradually, almost linearly, to a maximum value during the observation window. The SIF histories extracted from DGS data starting at the instant the healed crack initiated and then propagated slowly are shown in Fig. 9(b). Again, here $t = 0$ corresponds to crack initiation at the natural crack-tip produced after the wedge insertion into the notch. The mode-I SIF,K_I, (solid black symbols) increased steadily from much lower values to ~ 0.37 MPa$\sqrt{\text{m}}$ when the self-healed crack initiated. This is accompanied by an abrupt jump in the stress intensity factor to ~ 0.5 MPa$\sqrt{\text{m}}$ as the crack length suddenly increased from its shorter self-healed state to longer hairline crack state. Subsequently, the stress intensity factors for the natural crack increased almost linearly for the next 22 s until the crack initiated at the natural tip and grew slowly afterwards. During slow crack growth, the stress intensity factors are nearly constant, as indicated by the trend line. Interestingly, the DGS method is able to estimate the fracture toughness of the pre-crack even when the angular deflections are very small, approx. 10 to 20 μrad. The results are, however, relatively noisy due to the fact that the experiments were conducted without any vibration and thermal isolation of the optical setup.

In addition to SIF history, the energy release rate,$G = K_I^2/E$, was also evaluated and is shown in Fig. 10. The energy release rate increased until the healed crack initiated at ~ 2 J/m^2. Subsequently, G increased instantaneously (to approx. 3 J/m^2) due to the sudden opening of the self-healed crack. Afterwards, G increased to ~ 7 J/m^2 when it initiated at the natural crack-tip. Later, the crack continued to propagate in a mode-I fashion until the end of observation window with approximately the same value at initiation, as suggested by gray trend line.

3. Finite element model

A complementary finite element analysis was carried out for evaluating the fracture parameters at crack initiation and during slow crack growth. Components of WST assembly included the SLG specimen, steel pins and the wedge. The components like steel pins and the wedge (Young's modulus, $E = 200$ GPa) cannot be treated as rigid when compared to the stiffness of the specimen since SLG is also a relatively stiff material ($E = 70$ GPa) and has a high configurational stiffness in the WST geometry. Hence, upon loading, the strain energy gets stored in the steel pins and wedge as well the SLG specimen. To capture proper loading on the specimen in the setup as precisely as possible, the WST assembly was modeled for finite element analysis using Abaqus (Simulia, Rhode Island, USA) for performing a companion evaluation. Fig. 11 (a) shows the 2D geometric model. Due to symmetry, only one half of the model was considered. Fig. 11(b) shows the corresponding discretized model for FEA along with the symmetry boundary conditions. To implement self-healed crack, a total of 73 spring elements of type SPRING1 were used. These elements were connected from node (on the crack surface) to the ground and oriented normal to the crack flank. Interfaces between wedge and steel pins, SLG specimen and steel pins were modeled using contact pairs as shown in inset of Fig. 11(b). Since the steel pins are relatively stiff compared to specimen, pins were modeled as the master surface and specimen as the slave surface. All the master and slave surfaces were represented in red and magenta colors, respectively, as depicted in inset of Fig. 11(b). And, surface-to-surface contact was used to simulate all steel to steel, steel to SLG contact pairs with a coefficient friction of 0.1. To achieve convergence, finite

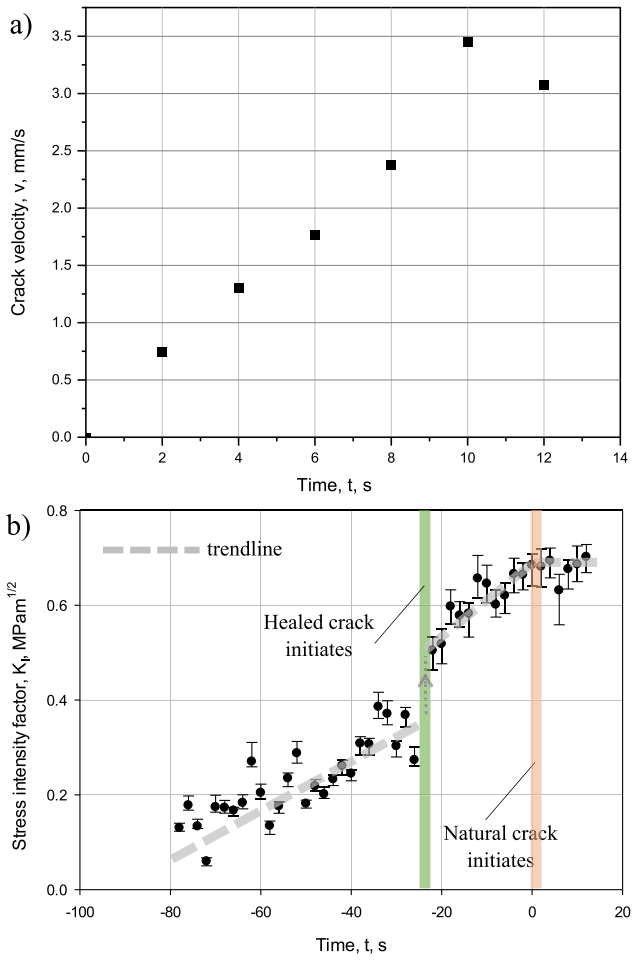

Fig. 9. (a) Crack velocity history and (b) stress intensity factor history for WST soda-lime glass specimen with a self-healed crack. (Time, $t = 0$ corresponds to crack initiation at natural crack-tip.).

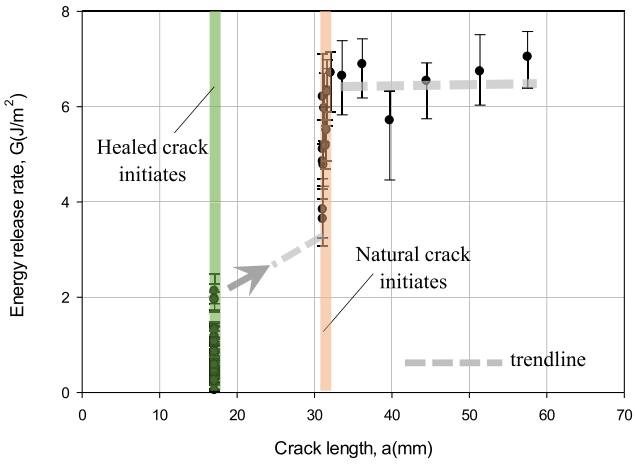

Fig. 10. Crack growth resistance behavior of self-healed crack in soda-lime glass.

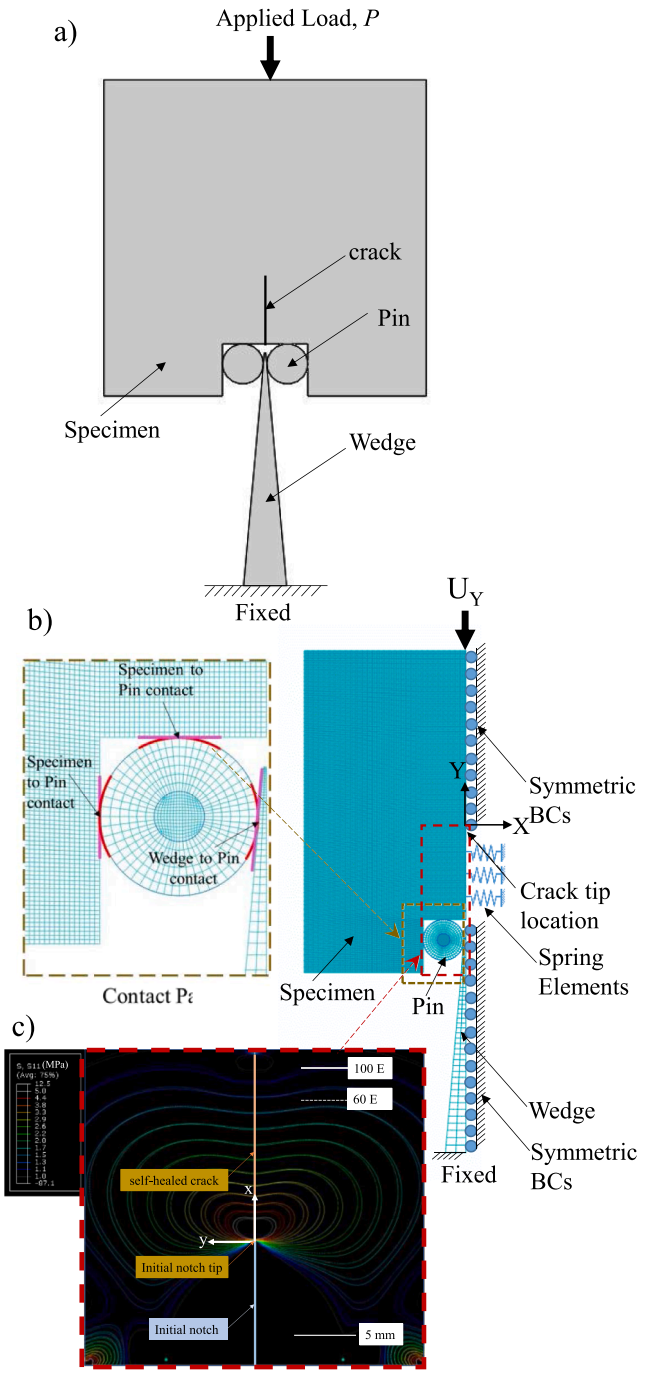

Fig. 11. Numerical model details for simulating the WST geometry: (a) 2D geometry and (b) 2D Finite Element Model with (c) σ_{yy} stress distribution at self-healed crack region.

displacements (0.01 mm on the pin and 0.05 mm on wedge) were imposed. Abaqus/CAE software was used by employing quadratic plane stress elements (CPS8R) for the soda-lime glass specimen, steel pins and the wedge. In total the model consisted of 31,000 elements and 93,000 nodes. Experimentally measured crosshead displacements at each time instant were imposed at the top loading point of the specimen. The bottom edge of the wedge was fully constrained and symmetric boundary conditions were applied on the line-of-symmetry of the specimen and wedge. The computed in-plane displacement field, u_y around the crack-tip under plane-stress condition was expressed using the asymptotic equation,

$$u_y = \sum_{N=1}^{\infty} \frac{1}{2\mu} A_N r^{N/2} \left\{ \left(\frac{3-\upsilon}{1+\upsilon} \right) sin\frac{N}{2}\theta + \frac{N}{2} sin\left(\frac{N}{2} - 2 \right)\theta - \left(\frac{N}{2} + (-1)^N \right) sin\frac{N}{2}\theta \right\} \quad (3)$$

In the above, (r, θ) denote the local crack-tip polar coordinates, and $r = \sqrt{x^2 + y^2}$ and $\theta = tan^{-1}\left(\frac{y}{x}\right)$ in the crack growth direction. The coefficient A_1 in the asymptotic series are related to the mode-I SIF as, $K_I = A_1\sqrt{2\pi}$. For analysis, the data near the crack-tip in the region $0.25 \leqslant r/B \leqslant 1.5$ behind the crack-tip were considered. Using the first 3 terms ($N = 3$) behind the crack-tip ($\theta = \pi$), Eq. (3) was simplified as,

$$Eu_y(r, \theta = \pi) = 4\left(\frac{K_I}{\sqrt{2\pi}} \right) r^{1/2} - 4r^{3/2}A_3 \quad (4)$$

The overdeterminstic least-squares analysis was performed using Eq. (4) to evaluate mode-I stress intensity factor, K_I. In Eq. (4), E is the modulus of elasticity of SLG.

To simulate self-healed crack in the specimen, spring elements (see, Fig. 11(b)) were used by assuming normal contact. The potential reduction in stiffness across the crack flanks due to self-healing was simulated by varying the elastic modulus of those spring elements. Furthermore, the stiffness of those springs was assumed to be uniform but varied from 100% to 40% of virgin SLG to simulate varying degrees of healing. Each case was simulated separately for the same applied far-field loading up to when the self-healed crack initiated in the experiments. The distribution of dominant stress σ_{yy} is shown in Fig. 11(c) as a representative case. The stress contours for the virgin material (100% E) appears to be greater when compared to the self-healed crack whose elastic modulus was chosen to be 60% of the virgin material. This indicates that the specimen experiences higher stress if the stiffness of self-healed crack is equal to that of the virgin material. The results for stress intensity factors are shown in Fig. 12(a). The mode-I stress intensity factor, K_I, increased monotonically in each case. Evidently, the rate of increase in K_I is noticeably affected by the choice of the stiffness of the crack flank contact elements. Upon overlaying each of these data sets on experimental counterparts, it was concluded that the simulation corresponding to approx. 60% of the virgin material modulus matched the experimental ones quite well. Thus, a 40% reduction in the elastic modulus due to self-healing appears to have occurred in the present case.

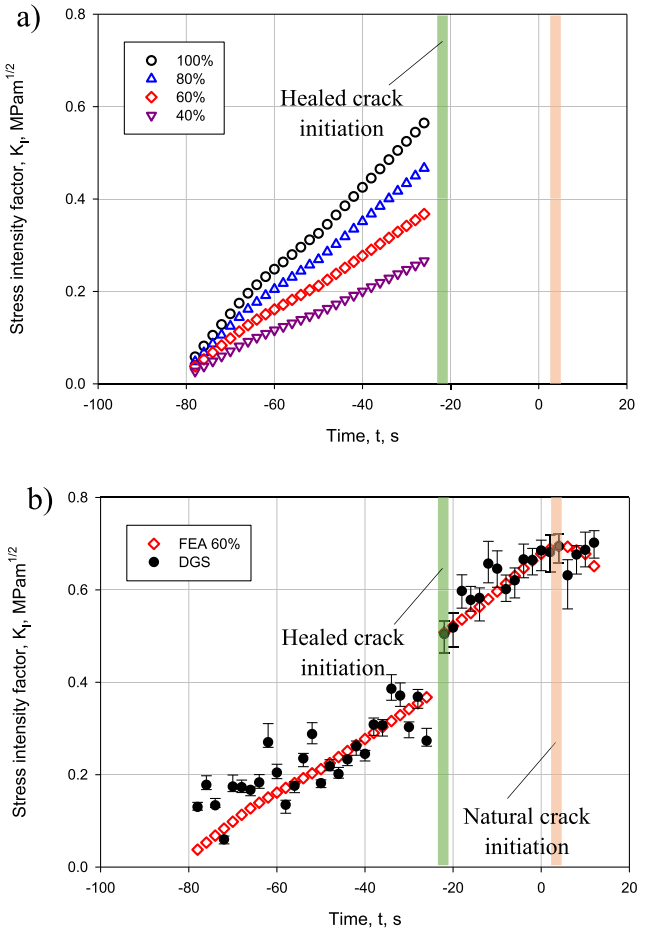

Fig. 12. Stress intensity factor histories from FEA: (a) SIF histories for different crack flank stiffness up to healed crack initiation, (b) SIF histories along with DGS experimental results for 60% stiffness. (Time, $t = 0$ corresponds to crack initiation at natural crack tip.).

Subsequently, the K_I values increased suddenly as in the experimental counterparts due to a jump in the crack length as the self-healed crack opened instantaneously. After initiation of the self-healed crack, the values increased again monotonically until the natural crack-tip initiated. The K_I value at the natural crack-tip was $\sim$ 0.7 MPa$\sqrt{m}$, close to the experimental counterpart. Once the crack initiated, it propagated and reduced to $\sim$ 0.65 MPa$\sqrt{m}$ by the end of the observation window. The K_I values from experiments and simulation show a good agreement.

4. Discussion

The crack initiation and slow crack growth characteristics of soda-lime glass containing a self-healed crack show that the mode-I stress intensity factors, K_I, of the self-healed crack increase until initiation at $\sim$ 0.37 MPa$\sqrt{m}$ under laboratory conditions. This value of fracture toughness of the self-healed crack measured here is far below that of virgin SLG, by a factor of nearly two. Thus, it should be a concern for the mechanical integrity of load bearing structures involving SLG due to the possibility of invisible self-healed cracks. These general observations and fracture parameter quantifications are rather consistent with prior works in the literature made using far field load/deflection measurements instead of full-field optical evaluations undertaken here. Wiederhorn and Townsend [1] studied slow crack growth in double cantilever beam specimens subjected to bending. They have reported an even lower critical stress intensity factor of $\sim$ 0.17 MPa$\sqrt{m}$ (20% of the value relative to the virgin material) and the corresponding fracture energy of $\sim 0.2 \pm 0.2$ J/m^2. Terry et al., [2] investigated self-healing of cracks in soda-lime glass using double-cleavage drilled-hole compression (DCDC) specimen. The strain energy release rate for reopening of the healed cracks was obtained as $\sim 1.7 \pm 0.2$ J/m^2 (and the critical K_I $\sim 0.34 \pm 0.02$ MPa$\sqrt{m}$).

This being an optical study of fracture characteristics of SLG in the presence of self-healed cracks, it is necessary to examine the results in the context of potential measurement errors. As DGS quantifies angular deflection of light rays that are proportional to two orthogonal stress gradients, there are potential sources of measurement errors including those due to crack-tip location and quantification of extremely small angular deflections of the order of 10 μrad. Due to the singular nature of these stress gradients at the crack-tip, the contours converge, as shown in the left column of Fig. 8, to the crack-tip. Hence, identification of the crack-tip is relatively straight forward and shown to be accurate to <

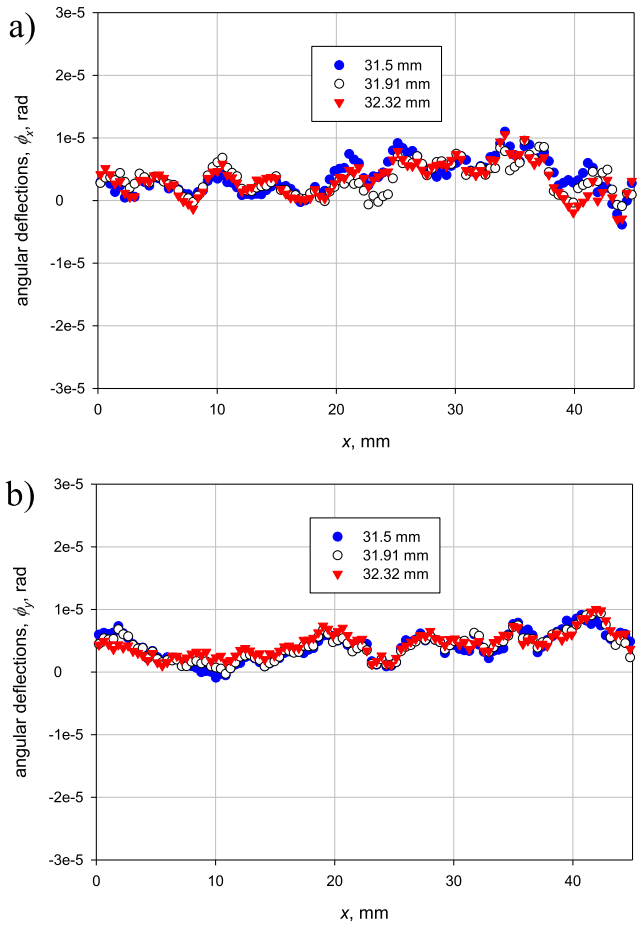

Fig. 13. Error assessment of angular deflections along three neighboring locations; (a) ϕ_x and (b) ϕ_y. ($x = 0$ corresponds to the upper loading point on WST geometry).

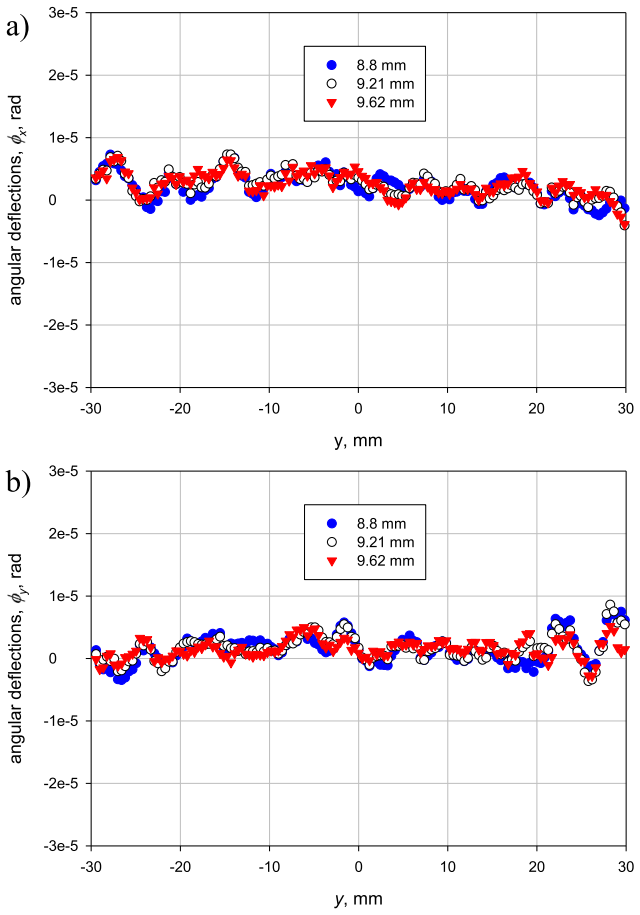

Fig. 14. Error assessment of angular deflections along three neighboring locations; (a) ϕ_x and (b) ϕ_y. ($y = 0$ corresponds to initial notch position.).

200 μm of positional error [11]. Furthermore, DGS is able to quantify them in the whole field even though the angular deflections of light rays caused by the stress-state around the crack-tip are very small. Fig. 9 shows experimental scatter in the stress intensity factor history of self-healed crack. The data before the initiation of the self-healed crack when the angular deflections of the light rays are relatively small when compared to those at later stages is worth examining more carefully. Noting that these experiments were conducted under nominal conditions in a lab situated on top floor of a four-story building without vibration isolation and in open circulating air. Thus, structural vibrations and thermal/air currents during experimentation contribute towards perturbation of lights rays and experimental scatter in the data. Hence, to ensure that the reported data trends are indeed reliable, two successive images, both in the undeformed state of the specimen, were correlated with each other and the resulting 'angular deflections' ϕ_x and ϕ_y are plotted in Fig. 13(a) and (b). These angular deflections values are considered along three neighboring vertical lines at 31.50 mm, 31.91 mm and 32.32 mm relative to the loading point on the WST geometry. It can be observed that, these values fluctuate in the range of 10 μrad instead of being zero expected under ideal conditions of no mechanical vibrations and thermal perturbations in the optical paths. Similar plots of ϕ_x and ϕ_y are shown Fig. 14(a) and (b) but along three neighboring horizontal lines located at 8.80 mm, 9.21 mm and 9.62 mm relative to the initial notch. Despite a few local peaks, the scatter in the data is well within 5 μrad. Hence, it is reasonable to conclude that a 10 μrad measurement accuracy from the optical setup and post-processing method used for measurements.

Another source of experimental scatter is associated with the evaluation of K_I from data in the *vicinity* of the crack-tip at different radial extents. Different data zones, $0.35 \le r/B \le 1.1$, $0.3 \le r/B \le 1.2$, $0.3 \le r/B \le 1.3$, $0.3 \le r/B \le 1.5$, and $0.25 \le r/B \le 1.5$, were used separately during least-squares analyses. The inner limit was to avoid data influenced by triaxial deformations whereas the outer limit was to prevent excessive far-field effects that influence the outcome due to the limited number of terms employed in the asymptotic stress field expression. The stress intensity factors were evaluated from all these regions separately and averaged. The scatter in the results are shown in Fig. 9(b) using error bars. The resulting fracture toughness of the self-healed crack-tip was 0.37 ± 0.03 MPa$\sqrt{\text{m}}$ (energy release rate of $\sim$ 1.8 J/m^2), far below the 0.7 MPa$\sqrt{\text{m}}$ for the virgin material. These suggest the robustness of the measurements presented in this work.

5. Conclusions

A somewhat obscure yet important issue of quasi-static fracture mechanics of soda-lime glass (SLG) with a self-healed crack was studied. The full-field optical method of digital gradient sensing or DGS was used to investigate the problem of crack initiation and slow growth from a self-healed crack in a SLG coupon. A WST specimen geometry with a pre-cut notch was adopted for experimentation. A mode-I natural hairline crack was generated by tapping a wedge into the notch that self-healed subsequently under ambient conditions upon retracting the wedge. The WST specimen with a self-healed crack was reloaded afterwards in a testing machine in a displacement controlled mode while monitoring the crack-tip region to quantify mechanical fields using DGS. DGS was able to quantify extremely small angular deflections of light rays, of the order of 10 μrad, due to the crack-tip state of stress under quasi-static

conditions without optical or mechanical isolation of the setup. Two orthogonal stress gradients, one parallel and the other perpendicular to the crack, were quantified in the entire region of interest. By performing least-squares analysis of the measured quantities, in conjunction with expressions for asymptotic stress gradient fields, the stress intensity factors and energy release rates at various stages of fracture were evaluated.

The experimental results indicate that the self-healed crack initiated at a critical stress intensity factor of ~ 0.37 MPa$\sqrt{\text{m}}$ and fracture toughness of 1.8 J/m^2. These values are far below that for the virgin SLG of ~ 0.7 MPa$\sqrt{\text{m}}$ and ~ 6.5 J/m^2, respectively, when the crack initiated from the natural hairline crack. This in turn suggests that structural design involving SLG needs to consider substantial degradation of fracture toughness in the presence of undetected self-healed cracks. A companion finite element analysis of the WST geometry with far-field displacements imposed on the specimen as boundary condition was also undertaken to supplement measurements. The self-healed crack was simulated using reduced contact stiffness across the healed crack flanks. The results show that a uniform 40% degradation of spring stiffness along the crack flanks was able to mimic the experimental trends well.

Declaration of Competing Interest

The authors declare that they have no known competing financial interests or personal relationships that could have appeared to influence the work reported in this paper.

Acknowledgements

The corresponding author is grateful to the support of the U.S. Army Research Office for sponsoring research on this topic, the most recent being through grant W911NF2210015.

References

[1] S.M. Wiederhorn, P.R. Townsend, Crack healing in glass, J. Am. Ceram. Soc. 53 (9) (1970) 486–489.
[2] T.A. Michalske, E.R. Fuller Jr, Closure and repropagation of healed cracks in silicate glass, J. Am. Ceram. Soc. 68 (11) (1985) 586–590.
[3] B. Stavrinidis, D.G. Holloway, Crack healing in glass, Phys. Chem. Glasses, 1983. 24(1): p. 19-25.
[4] S.M. Wiederhorn, Subcritical crack growth in ceramics, Fract. Mech. Ceram. (1974) 613–646.
[5] D. Munz, T. Fett, Ceramics: mechanical properties, failure behaviour, materials selection, Springer Science & Business Media, 1999.
[6] S.M. Wiederhorn, Influence of water vapor on crack propagation in soda-lime glass, J. Am. Ceram. Soc. 50 (8) (1967) 407–414.
[7] T. To, F. Célarié, C. Roux-Langlois, A. Bazin, Y. Gueguen, H. Orain, M. Le Fur, V. Burgaud, T. Rouxel, Fracture toughness, fracture energy and slow crack growth of glass as investigated by the Single-Edge Precracked Beam (SEPB) and Chevron-Notched Beam (CNB) methods, Acta Mater. 146 (2018) 1–11.
[8] D. Ferretti, M. Rossi, G. Royer-Carfagni, An ESPI experimental study on the phenomenon of fracture in glass. Is it brittle or plastic? J. Mech. Phys. Solids 59 (7) (2011) 1338–1354.
[9] B.K. Singh, D.S. Mehta, P. Senthilkumaran, Interferometric visualization of crack growth in glass plate, Appl. Phys. B 125 (2) (2019) 21.
[10] B.M. Sundaram, H.V. Tippur, Full-field measurement of contact-point and crack-tip deformations in soda-lime glass. Part-I: Quasi-static Loading, Int. J. Appl. Glass Sci. 9 (1) (2018) 114–122.
[11] B.M. Sundaram, H.V. Tippur, Dynamic fracture of soda-lime glass: A full-field optical investigation of crack initiation, propagation and branching, J. Mech. Phys. Solids 120 (2018) 132–153.
[12] S. Dondeti, H.V. Tippur, A comparative study of dynamic fracture of soda-lime glass using photoelasticity, digital image correlation and digital gradient sensing techniques, Exp. Mech. 60 (2) (2020) 217–233.
[13] S. Dondeti, H.V. Tippur, Cascading crack bifurcations in soda-lime glass: Quantification of fracture mechanics-based precursors using Digital Gradient Sensing, Int. J. Solids Struct. 234 (2021), 111252.
[14] H. Harmuth, K. Rieder, M. Krobath, E. Tschegg, Investigation of the nonlinear fracture behaviour of ordinary ceramic refractory materials, Mater. Sci. Eng., A 214 (1–2) (1996) 53–61.
[15] E. Brühwiler, F.H. Wittmann, The wedge splitting test, a new method of performing stable fracture mechanics tests, Eng. Fract. Mech. 35 (1–3) (1990) 117–125.
[16] S. Korte, V. Boel, W. De Corte, G. De Schutter, Static and fatigue fracture mechanics properties of self-compacting concrete using three-point bending tests and wedge-splitting tests, Constr. Build. Mater. 57 (2014) 1–8.
[17] R. Walter, L. Østergaard, J.F. Olesen, H. Stang, Wedge splitting test for a steel–concrete interface, Eng. Fract. Mech. 72 (17) (2005) 2565–2583.
[18] R. Vargas, J. Neggers, R.B. Canto, J.A. Rodrigues, F. Hild, Analysis of wedge splitting test on refractory castable via integrated DIC, J. Eur. Ceram. Soc. 36 (16) (2016) 4309–4317.
[19] Y. Dai, D. Gruber, H. Harmuth, Determination of the fracture behaviour of MgO-refractories using multi-cycle wedge splitting test and digital image correlation, J. Eur. Ceram. Soc. 37 (15) (2017) 5035–5043.
[20] C. Periasamy, H.V. Tippur, Measurement of orthogonal stress gradients due to impact load on a transparent sheet using digital gradient sensing method, Exp. Mech. 53 (1) (2013) 97–111.